Spectroscopic, structural and theoretical studies of 2-methyl-4-nitroaniline (MNA) crystal. Electronic transitions in IR

ARTICLE *in* JOURNAL OF RAMAN SPECTROSCOPY · JUNE 2008

Impact Factor: 2.67 · DOI: 10.1002/jrs.1924

6 AUTHORS, INCLUDING:

Maria Magdalena Szostak
Wyższa Szkoła Handlowa we Wrocławiu
35 PUBLICATIONS **262** CITATIONS
SEE PROFILE

Tomasz Misiaszek
Wroclaw University of Technology
17 PUBLICATIONS **177** CITATIONS
SEE PROFILE

Ireneusz Natkaniec
Joint Institute for Nuclear Research
84 PUBLICATIONS **404** CITATIONS
SEE PROFILE

Andrzej Pawlukojć
Joint Institute for Nuclear Research
67 PUBLICATIONS **542** CITATIONS
SEE PROFILE

JOURNAL OF RAMAN SPECTROSCOPY
J. Raman Spectrosc. 2008; **39**: 849–862
Published online 2 June 2008 in Wiley InterScience
(www.interscience.wiley.com) DOI: 10.1002/jrs.1924

JRS

Spectroscopic, structural and theoretical studies of 2-methyl-4-nitroaniline (MNA) crystal. Electronic transitions in IR

U. Okwieka,[1] M. M. Szostak,[1]* T. Misiaszek,[1] I. Turowska-Tyrk,[1] I. Natkaniec[2,3] and A. Pavlukojć[2,4]

[1] Institute of Physical and Theoretical Chemistry, Wrocław University of Technology, Wybrzeże Wyspiańskiego 27, 50-370 Wrocław, Poland
[2] Joint Institute of Nuclear Research, 141980 Dubna, Russia
[3] H. Niewodniczański Institute of Nuclear Physics, Radzikowskiego 152, 31-342 Kraków, Poland
[4] Institute of Nuclear Chemistry and Technology, Dorodna 16, 03-195 Warszawa, Poland

Polarized FT-IR, Raman, neutron scattering (IINS), and UV-Vis-NIR spectra of 2-methyl-4-nitroaniline (MNA) crystal plates, powder, and solutions were measured in the 10–50 000 cm^{-1} range. The FT-IR spectrum of deuterated MNA (DMNA) in KBr pellet, the Raman spectrum of the DMNA powder as well as the EPR spectrum of the MNA powder were also recorded. Complete assignments of bands to normal vibrations have been proposed. Density functional theory (DFT) calculations of wavenumbers and potential energy distribution (PED) have been performed to strengthen the assignments. The analysis of vibrational and electronic spectra has revealed vibronic couplings in MNA molecules in solutions and in crystals. In the polarized FT-IR spectra of the crystal five unusually large bands are observed in MIR and NIR regions. Their origin is discussed in terms of N–H···O, C–H···O, C–H···H–N hydrogen bonds, intermolecular charge transfers, electrostatic interactions, and ion radicals formation in the crystal. The role of a methyl group introduction to 4-nitroaniline is analyzed. The crystal structure of MNA at the room temperature was re-investigated. Copyright © 2008 John Wiley & Sons, Ltd.

KEYWORDS: vibrational spectra; NLO crystal; electronic transitions in IR; ion radicals; hydrogen bonds

INTRODUCTION

Molecular packing as well as intra- and intermolecular interactions are crucial for understanding functional properties of solids. Their knowledge enables us to predict the relationship between microscopic and macroscopic properties and to develop new materials. Spectroscopic methods are well established tools for such studies.

The substitution of a methyl group to 4-nitroaniline (p-NA), a push–pull model compound in nonlinear optics, delivered material with enhanced optical nonlinearity. 2-methyl-4-nitroaniline (MNA) crystallizes in the noncentrosymmetric monoclinic Cc structure.[1] MNA crystals exhibit a large figure of merit for second harmonic generation (SHG), almost 2000 times larger than that for lithium niobate,[1] and strong Pockels effect.[2]The intramolecular charge transfer (ICT) from the electron donating $-NH_2$ group, through highly polarizable benzene ring, to the electron withdrawing $-NO_2$ group is considered as the general cause of optical nonlinearity in push–pull molecules.[3] The crystal structure of MNA has been reported;[1,2,4] however its vibrational spectra have not yet been analyzed in detail. FT-IR spectra of crystalline MNA deposited on a poly(tetrafluoroethylene) (PTFE) substrate were studied by Vallée *et al*.[5,6] They assigned the most intense bands on the basis of *ab initio* calculations.[6] Nogueira *et al*.[7] reported the longitudinal optical (LO) and transversal optical (TO) wavenumbers of polar vibrations found in the unpolarized FT-IR reflectivity spectra of MNA crystals. Some information on electronic states of the MNA molecule in the crystal can be extracted from visible transmission[1] and polarized reflectance and electroreflectance spectra[8]of single crystals. Intra- and intermolecular electronic transitions were calculated for MNA molecular clusters.[9] Calculated singlet and triplet electronic transitions of single MNA molecule and a doublet transition of its radical anion in the gas phase were recently reported together with the low-temperature photoemission spectra of MNA crystals.[10]

*Correspondence to: M. M. Szostak, Institute of Physical and Theoretical Chemistry, Wrocław University of Technology, Wybrzeże Wyspiańskiego 27, 50-370 Wrocław, Poland.
E-mail: magdalena.m.szostak@pwr.wroc.pl

By investigation of the MNA crystals we continue our spectroscopic (IR, Raman, and electronic) studies on the optically nonlinear molecular crystals such as 3-aminophenol,[11] 3-nitroaniline (m-NA),[12,13] and 4-izopropylphenol (4-IP).[14] We succeeded with obtaining MNA single crystal thin plates of good optical quality suitable for recording polarized FT-IR spectra and for analysis of dichroic ratios of bands. Raman, incoherent inelastic neutron scattering (IINS), and electronic spectra of MNA crystalline layer as well as IR, Raman, and UV-Vis spectra of MNA solutions and of a deuterated 2-methyl-4-nitroaniline (DMNA) were also measured to collect complementary data. Electronic spectra enable interpretation of vibrational spectra in terms of vibronic theories of IR[15] and Raman[16] intensities. The striking appearance of five very large massifs in the polarized IR spectra of the MNA crystal, similar to electronic transition bands observed in IR spectra of polyacene radical anions,[17] provoked us to measure an electron permagnetic resonance (EPR) spectrum of the solid MNA. The occurrence of paramagnetic species absorbing in NIR and/or generated by NIR was previously found in m-NA crystals.[18–21]

The crystal structure of MNA was determined by X-ray diffraction at room temperature by Levine *et al*.[1] and 1 year later by Lipscomb *et al*.[2] The structure was also studied by Howard *et al*.[22] (X-ray) at 125 K and later by Whitten *et al*.[23] at 100 K (joined X-ray and neutron diffraction measurements), in both papers, in order to assess the molecular dipole moment in the MNA crystal. Ferguson *et al*.[4]determined the MNA crystal structure at 150 K by X-ray method. Because of observed differences between determined parameters of the crystal structures reported in works cited above and because all our measurements were performed at room temperature we solved the crystal structure at 298 K.

The aim of this work was to determine and rationalize manifestations of intra- and intermolecular interactions in optical and neutron scattering spectra of MNA. The role of the weak electron donor methyl group in changing the MNA crystal packing and interactions was also studied.

EXPERIMENTAL AND CALCULATION METHODS

Commercial, yellow MNA (Aldrich) was purified by threefold vacuum sublimation. Monocrystalline samples were obtained from water–methanol (1 : 2 v/v) solutions by slow evaporation of the solvent at room temperature. Maximum dimensions of the crystal plates were about $0.5 \times 0.3 \times 0.05$ cm^3 and they grew in direction perpendicular to the crystallographic **b** axis, i.e. in the (010) plane. X-ray diffraction measurements were performed on a KUMA diffraction KM4CCD four-circle automatic diffractometer equipped with an area detector. Single crystal and molecular structures of MNA were examined with a KM4CCD data reduction. The SHELXS97 and SHELXL97 programs were used to solve and refine the structure. Determined parameters of the crystal structure of MNA are close to those of Ferguson *et al*.[4] It is important to mention that the **a** and **c** axes in our structure correspond to the **c** and **a** axes in Ref. 2, respectively. The (010) plane of monoclinic crystals contains two main dielectric axes X and Z which are observed as extinction directions under a polarizing microscope with crossed polarizers.[24] The two directions in the MNA crystal were found in the manner described in Ref. 24. Samples oriented in such a way were used to measure the FT-IR spectra with electric vector **E** of beam parallel to the X and Z directions. These axes are nearly parallel or perpendicular to the benzene ring planes of MNA molecules (Fig. 1). The Y dielectric axis is parallel to the **b** crystallographic axis. Distinction between X and Z directions in the MNA crystal as well as their orientation with respect to the crystallographic axes and edges of the crystal plate were made according to

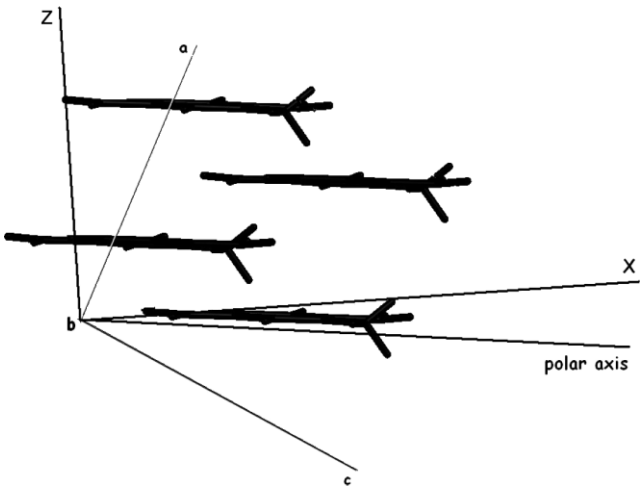

Figure 1. The schematic view of the MNA crystal along the **b** axis. Relative orientation of dielectric and crystallographic axes is indicated (according to Ref. 2).

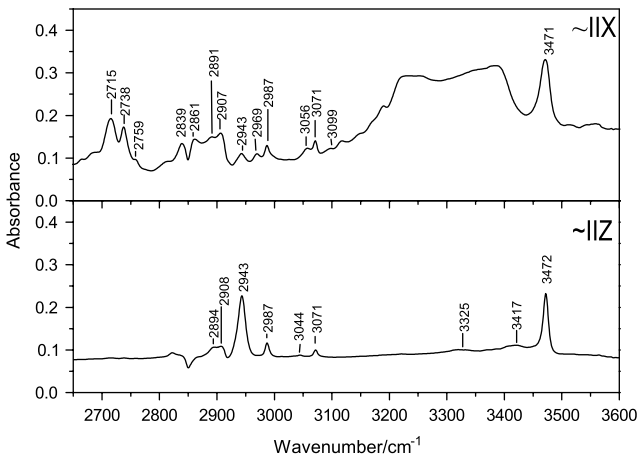

Figure 2. Polarized FT-IR spectra of the monocrystalline MNA plate.

DOI: 10.1002/jrs

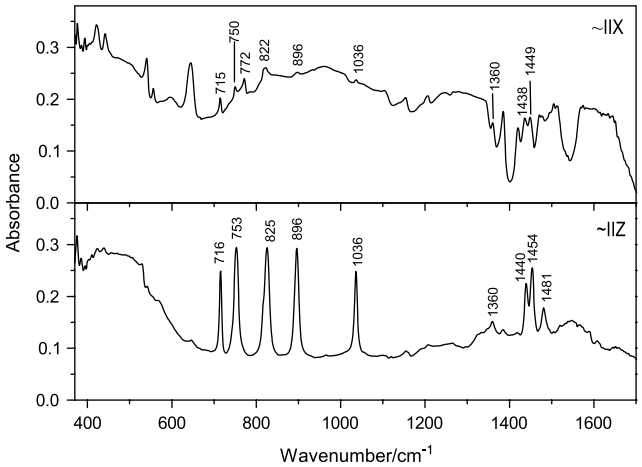

Figure 3. Polarized FT-IR spectra of the monocrystalline MNA plate.

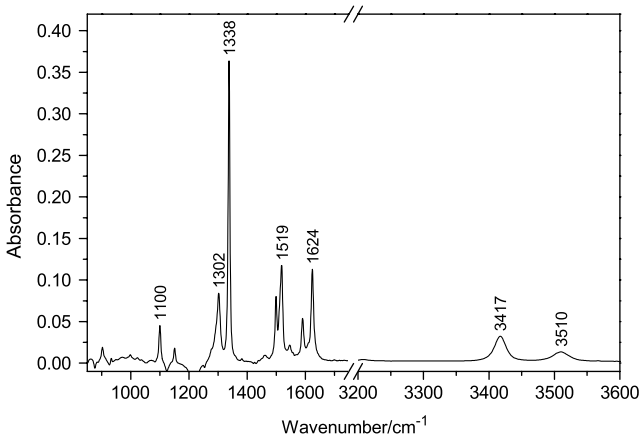

Figure 4. FT-IR spectrum of the MNA solution in $CHCl_3$.

data given in Ref. 2 but after taking into account the **a** and **c** axes inversion.

FT-IR spectra were recorded on a Perkin Elmer FT-IR 2000 spectrometer at 4 cm^{-1} resolution. The polarized absorption (transmission) spectra measured for the thinnest plates in the MIR region (370–4000 cm^{-1}) are presented in Figs. 2 and 3. Spectra of MNA solutions in $CHCl_3$ (~0.5% w/w and 0.062-mm cell thickness) and in CCl_4 (saturated, 0.512-mm cell) were also measured in the MIR region. Since both spectra are very similar, only one in $CHCl_3$ is shown in Fig. 4. The far IR (FIR, 50–700 cm^{-1}) spectrum was recorded for MNA suspension in nujol (Fig. 5). In the same figure the corresponding Raman spectrum is given. Raman spectra of powdered MNA and deuterated MNA (DMNA; 85% ND_2) excited with the 514.5-nm line (shown together in Fig. 6) and polarized Raman spectra of the 0,5% w/w MNA solution in $CHCl_3$ (not shown) excited with the 514.5-nm line of a spectra physics Ar–Kr ion laser, were recorded on a Jobin-Yvon T 64000 spectrograph equipped with a liquid N_2 cooled CCD camera at spectral resolution 2 cm^{-1}. Integrated intensities of bands measured at parallel (vertical–vertical, VV) and perpendicular (vertical–horizontal, VH) polarizations were the basis for determination of experimental depolarization ratios. FT-IR spectra of MNA and DMNA in KBr pellet were also measured (Fig. 7). UV-Vis spectra of MNA solutions in ethanol and methanol (concentration ~10^{-4} M) as well as those of the saturated solutions in water, isooctane, tetrahydrofurane, chloroform, and acetone – all solvents spectroscopically pure – were measured on a Shimadzu 2101 PC spectrophotometer. UV-Vis–NIR reflection spectra, transformed into absorption, were recorded on a Cary 500 Scan UV-Vis–NIR (Varian) apparatus for the thin film of

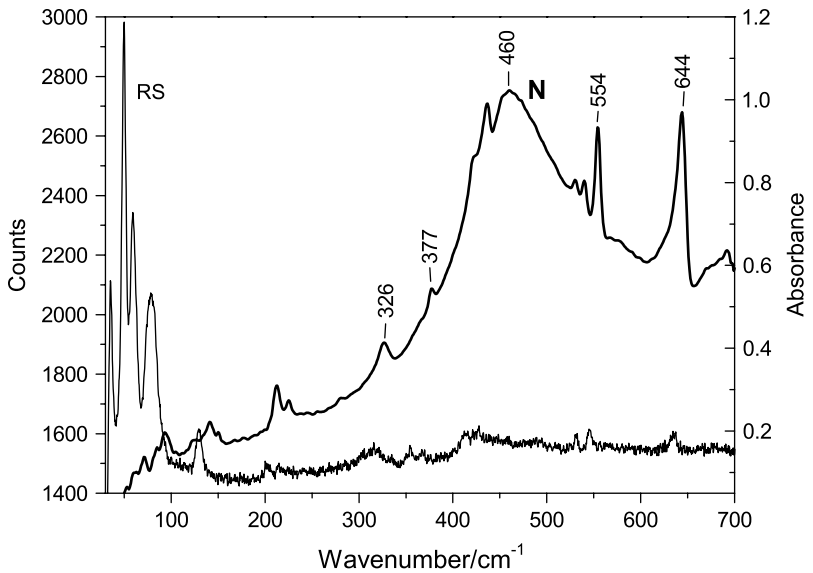

Figure 5. FT-IR spectrum of MNA in nujol suspension (N) and Raman spectrum ($\lambda_{exc} = 514.5$ nm) of powdered MNA (RS). Low wavenumber range.

DOI: 10.1002/jrs

JRS

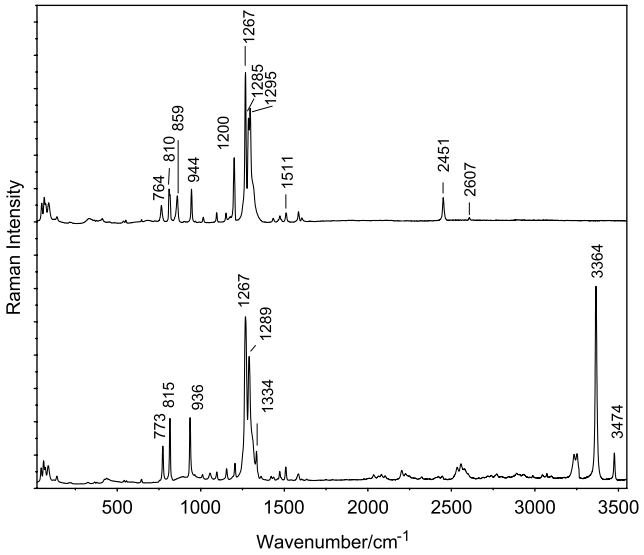

Figure 6. Raman spectra of powdered MNA (bottom) and deuterated MNA analogue (top) ($\lambda_{exc} = 514.5$ nm).

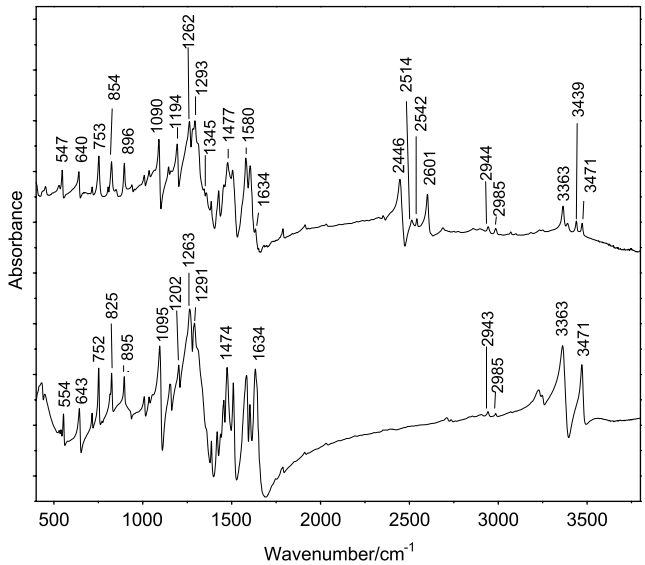

Figure 7. FT-IR spectra of deuterated MNA (DMNA) in KBr pellet (top). The MNA spectrum in KBr pellet is shown for comparison (bottom).

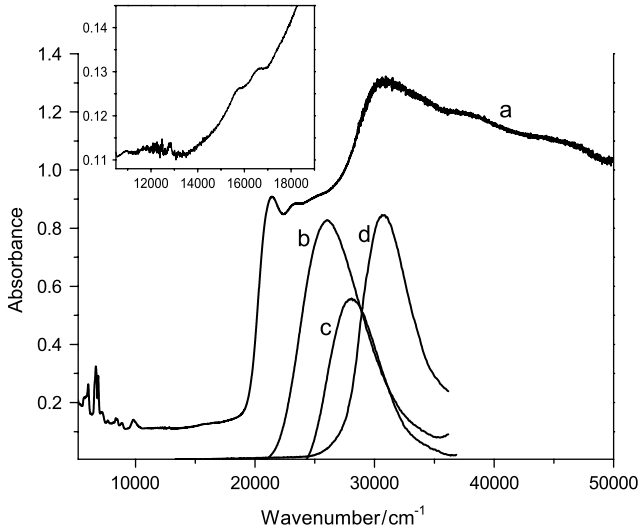

Figure 8. The UV-Vis-NIR spectra of the thin MNA layer (a) and of solutions in water (polar) (b), chloroform (medium polar) (c) and isooctane (nonpolar) (d).

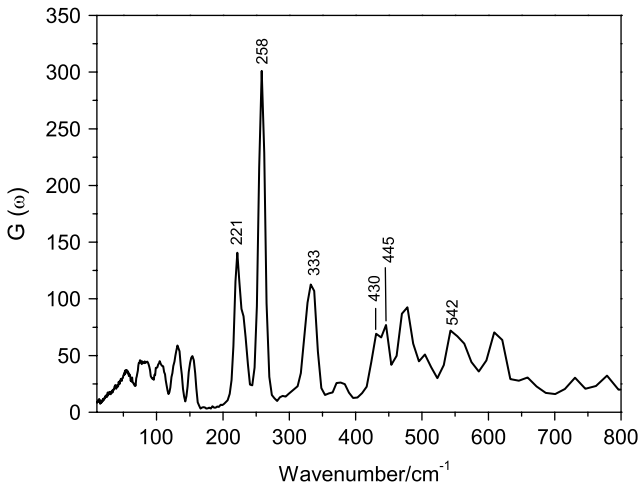

Figure 9. IINS spectrum of MNA powder at 20 K.

MNA layered on a quartz slide. The electronic spectra of the solid MNA and of the three selected solutions of MNA are shown in Fig. 8. Neutron diffraction and inelastic incoherent neutron scattering (IINS) spectra of powdered MNA were measured at 20 K (Fig. 9) and 290 K at 56.6° and 134.9° scattering angles using an inverted time-of-flight spectrometer NERA-PR. The resolution of this spectrometer in the 40–800 cm^{-1} range is comparable with optical spectrophotometers. The spectrometer is coupled with the IBR reactor in Joint Institute of Nuclear Research, Dubna, Russia. Additionally, in Fig. 10, the X and Z polarized FT-IR spectra are shown in the whole measured region to emphasize the difference in these spectra in the two polarizations.

Fully optimized ground state geometry, force field, and harmonic vibrational wavenumbers of the MNA molecule were calculated with the B3LYP/6-31++G(d,p) method implemented in Gaussian 2003.[25] The transformation of the force field from Cartesian to internal coordinates, recommended by IUPAC,[26] was carried out. Force constants determined by the above methods were used to calculate vibrational potential energy distribution (PED) among the normal coordinates. The harmonic vibrational wavenumbers are presented without any scaling.

DOI: 10.1002/jrs

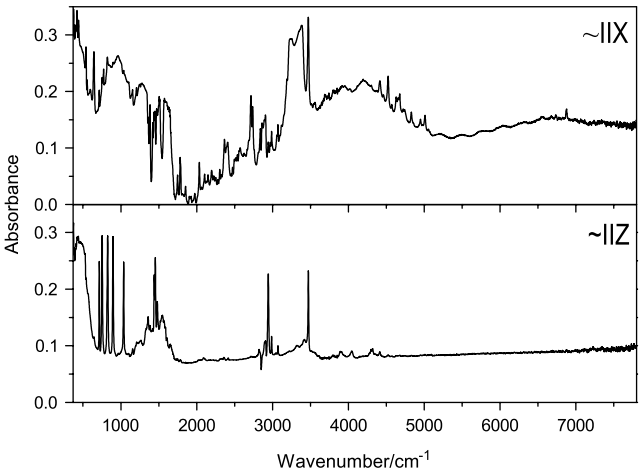

Figure 10. Polarized FT-IR spectra of monocrystalline MNA plate in MIR and NIR regions.

GROUP THEORY ANALYSIS

The MNA molecule contains 19 atoms; thus, assuming C_s symmetry point group, 35 modes of A′ symmetry and 16 of A″ symmetry should appear as bands in the spectra.

Further division into stretching (ν), in-plane bending (δ) and out-of-plane bending (γ) modes is as follows:

$$\begin{aligned}\Gamma = {} & 9a'(5\nu_{CC}, 4\delta_{CC}) + 3a''(3\gamma_{CC}) \\ & + 6a'(3\nu_{CH}, 3\delta_{CH}) + 3a''(3\gamma_{CH}) \\ & + 4a'(2\nu_{CN}, 2\delta_{CN}) + 2a''(2\gamma_{CN}) \\ & + 4a'(2\nu_{NO}, 2\delta_{NO_2}) + 2a''(2\gamma_{NO_2}) \\ & + 4a'(2\nu_{NH}, 2\delta_{NH_2}) + 2a''(2\gamma_{NH_2}) \\ & + 2a'(\nu_{C-CH3}, \delta_{C-CH3}) + a''(\gamma_{C-CH3}) \\ & + 6a'(3\nu_{CH_3}, 3\delta_{CH_3}) + 3a''(3\gamma_{CH3})\end{aligned}$$

Calculated and observed bands positions in the IR and Raman spectra of MNA solutions, observed and calculated depolarization ratios as well as computed PED values are compiled in Table 1. In Table 2 band positions found in the spectra of solid MNA, calculated and observed dichroic ratios as well as proposed assignments are collected. As in the Varsányi monograph[27] the Wilson notation of benzene modes has been applied in this paper.

The correlation diagram for the MNA crystal is shown in the scheme below.

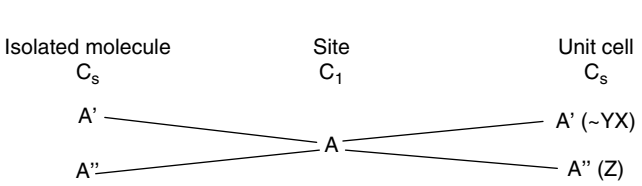

From the correlation diagram it results that every vibration of the MNA molecule in the crystal splits into two vibrations, both IR and Raman active. The two components of each of the split vibrations have transition dipole moments parallel (A′) and perpendicular (A″) to the X dielectric axis thus they can be observed in polarised IR spectra measured by us. This type of splitting is called Davydov (correlation) splitting and is due to the coupling between the translationally nonequivalent molecules in the unit cell.

ORIENTED GAS MODEL (OGM)

To calculate the theoretical dichroic ratios $R_{X/Z}$ of IR bands we have used the oriented gas model (OGM).[29] In this model the relative intensities of bands measured in two perpendicular directions can be calculated from the equation:

$$R_{X/Z} = \frac{n_Z}{n_X \cos\xi} \frac{\sum_{j=1}^{N} \cos^2(M_j, E_X)}{\sum_{j=1}^{N} [\cos\xi \cos(M_j, E_Y) \pm \sin\xi \cos(M_j, E_Z)]^2} \quad (1)$$

where n_X, n_Z are refractive indices for the two directions, (M_j, E_i) is the angle between the transition dipole moment vector $\mathbf{M_j}$ of a given vibration and the electric vector of the electromagnetic wave along the i direction (i = X, Y, Z, indicatrix axes), ξ is the angle between the **E** and **D** (displacement) vectors of the electromagnetic wave propagating through the crystal.

Values of the directional cosines of the transition dipole moments **M** (abbreviated here as tdm) were calculated immediately from the structural data. Coordinates of atoms in the MNA molecule were transformed from orthogonal abc* to the main dielectric XYZ axes system. For vibrations of A″ symmetry type, the tdm were assumed to be parallel to the normal to molecular plane. The planes of the phenyl ring, nitro and amine groups were considered separately. In the case of vibrations symmetrical with respect to the molecular plane (A′ symmetry type) directional cosines of tdm were replaced by the minus sines of an angle between **n** normal to the plane and the direction of **E**, i.e. $-\sin(\mathbf{n}, \mathbf{E}_i)$.[29] Exceptions were stretching symmetric and antisymmetric vibrations of amine and nitro groups for which tdm were calculated, respectively, as a geometrical sum and a difference of bonds treated as vectors. The sum in Eqn (1) runs over all N molecules in the unit cell. N equals to 4 in the MNA crystal. The refractive indices were calculated for $\lambda = 1100$ nm from Sellmeir's equation reported for the MNA crystal[30] and they are equal to $n_x = 1.7574$, $n_y = 1.5103$, $n_z = 1.3575$. The ξ angle in MNA crystals is almost 0°, like in the p-NA crystal,[29] thus Eqn (1) becomes:

$$R_{X/Z} = \frac{n_Z}{n_X} \frac{\sum_{j=1}^{4} [\cos(M, E_X)]^2}{\sum_{j=1}^{4} [\cos(M, E_Z)]^2} \quad (2)$$

DOI: 10.1002/jrs

Table 1. The comparison of theoretical wavenumbers, IR intensities, Raman activities, and depolarization degrees of bands and observed in spectra of MNA solutions. The potential energy distributions are given in local coordinates

Calculated wavenumbers [cm^{-1}]	ν_{IR} Solution in $CHCl_3$ [cm^{-1}]	ν_R Solution in $CHCl_3$, Polarization [cm^{-1}]		Depolarization degree		IR intensity [km mol^{-1}]	Raman activity [$Å^4$/amu]	PED's (in %)[a]
		VH[b]	VV[b]	Calc.[c]	Exp.[d]			
1	2	3	4	5	6	7	8	9
3717	3515w	–	–	0.75	–	29.1	57.6	$\nu^{as}_{NH_2}$ (100)
3604	3417m	3425vw	3425vw	0.16	0.37	52.5	296.3	$\nu^{s}_{NH_2}$ (100)
3246	–	–	–	0.23	–	1.9	72.3	ν_{CH} (98)
3232	–	–	–	0.28	–	1.4	50.4	ν_{CH} (99)
3185	–	–	–	0.31	–	13.3	111.9	ν_{CH} (98)
3135	–	–	–	0.68	–	9.8	54.8	ν_{CH_3} (91)
3068	–	–	–	0.64	–	18.4	101.1	ν_{CH_3} (94)
3017	–	–	–	0.10	–	35.3	229.5	ν_{CH_3} (99)
1675	1624m	1630vw	1628w	0.57	0.53	238.0	83.5	$\delta^{s}_{NH_2}$ (48)
1656	–	–	–	0.75	–	29.8	12.4	$\delta^{s}_{NH_2}$ (29), ν_{CC} (16)
1640	1589m	1594w	1596w	0.55	0.41	77.1	68.7	ν_{CC} (55)
1586	1519m	–	–	0.67	–	208.0	21.4	$\nu^{as}_{NO_2}$ (67)
1538	1499m	–	–	0.63	–	63.6	5.3	δ_{CH} (33), $\nu_{C-N(H_2)}$ (11)
1510	–	1467w	1467w	0.74	0.13	2.4	4.0	δ_{CH_3} (64)
1492	–	1425vw	1427vw	0.74	0.68	9.9	9.7	δ_{CH_3} (92)
1464	–	–	–	0.51	–	6.9	14.2	ν_{CC} (24), δ_{CH_3} (22)
1424	–	–	–	0.40	–	2.4	13.1	δ_{CH_3} (82)
1376	1333vs	1336vs	1336vs	0.33	0.29	564.9	587.8	$\nu^{s}_{NO_2}$ (63), $\nu_{C-N(O_2)}$ (16), $\delta^{s}_{NO_2}$ (15)
1394	1318vs	1316m	1316m	0.26	0.6	1.5	6.1	ν_{CC} (48)
	1302m	1300sh	1300sh	–	–	–	–	?
1336	1288sh	1284sh	1284sh	0.21	–	231.6	105.7	$\nu_{C-N(H_2)}$ (43), δ_{CH} (20)
1305	1278m	1278m	1279m	0.66	–	2.8	0.1	δ_{CH} (70)
1224	–	–	–	0.27	–	23.3	50.1	ν_{C-CH_3} (31), δ_{CC} (27)
1177	1154w	1160vw	1158vw	0.40	–	18.2	1.9	δ_{CH} (69), ν_{CC} (15)
1123	1100w	1104w	1104w	0.19	0.65	92.0	28.0	δ_{CH} (24), ν_{CC} (27), $\nu_{C-N(O_2)}$ (18)
1066	–	–	–	0.59	–	2.8	2.9	$\delta^{as}_{NH_2}$ (49), ν_{CC} (19)
1062	–	–	–	0.68	–	1.3	0.2	δ_{CH_3} (69)
1016	–	–	–	0.32	–	5.1	1.4	δ_{CH_3} (63), ν_{CC} (10)
972	–	–	–	0.75	–	0.9	0.1	γ_{CH} (85)
950	–	–	939vw	0.10	–	15.7	10.5	$\nu_{C-N(O_2)}$ (18), δ_{CC} (15), $\nu_{C-C(H_3)}$ (13)
928	–	–	–	0.49	–	13.5	0.1	γ_{CH} (80)
834	–	–	–	0.49	–	25.9	0.1	γ_{CH} (70), $\gamma_{C-N(H_2)}$ (10)
823	–	820vw	820vw	0.24	–	10.6	3.5	$\delta^{s}_{NO_2}$ (47), δ_{CC} (22)
781	–	–	774w	0.10	–	5.9	38.0	ν_{CC} (29) $\nu_{C-C(H_3)}$ (17), $\nu_{C-N(H_2)}$ (10)
747	–	–	–	0.65	–	23.1	0.9	γ_{NO_2} (inv) (56), γ_{CC} (18), $\gamma_{C-N(O_2)}$ (15)
707	–	–	–	0.66	–	1.2	0.5	γ_{CC} (52), γ_{C-NH_2} (22)
656	–	–	–	0.72	–	6.1	3.3	δ_{CC} (53), $\delta^{s}_{NO_2}$ (15)
557	–	–	–	0.66	–	2.9	4.5	$\delta^{as}_{NO_2}$ (37), $\delta_{C-N(O_2)}$ (20), $\delta_{C-N(H_2)}$ (16)
549	–	–	–	0.34	–	0.7	4.1	δ_{CC} (29), $\delta^{as}_{NO_2}$ (13)

Table 1. (*Continued*)

Calculated wavenumbers [cm^{-1}]	ν_{IR} Solution in $CHCl_3$ [cm^{-1}]	ν_R Solution in $CHCl_3$, Polarization [cm^{-1}] VH[b]	VV[b]	Depolarization degree Calc.[c]	Exp.[d]	IR intensity [km mol^{-1}]	Raman activity [$Å^4$/amu]	PED's (in %)[a]
1	2	3	4	5	6	7	8	9
539	–	–	–	0.29	–	5.8	1.8	γ_{CC} (45), $\gamma_{C-N(O_2)}$ (21), $\gamma_{C-N(H_2)}$ (11)
470	–	–	–	0.44	–	237.1	24.8	γ_{NO_2} (inv) (53) γ_{CC} (14)
442	–	–	–	0.37	–	98.4	6.8	γ_{CC} (49), $\gamma_{CC(H_3)}$ (17), γ_{NH_2} (inv) (12)
416	–	–	–	0.52	–	2.9	2.9	δ_{C-NH_2} (30), $\delta^{as}_{NO_2}$ (22), δ_{CC} (16)
366	–	–	–	0.12	–	3.8	2.7	δ_{CC} (38), $\nu_{C-N(O_2)}$ (21), γ_{NH_2} (twist) (18)
364	–	–	–	0.63	–	45.3	1.9	γ_{NH_2} (twist) (60), γ_{NH_2} (inv) (12)
315	–	–	–	0.65	–	5.6	0.8	δ_{CC} (22), $\delta_{C-N(O_2)}$ (13), $\gamma_{C-(O_2)}$ (12)
308	–	–	–	0.72	–	5.0	1.0	δ_{CC} (19), $\gamma_{C-N(O_2)}$ (14), $\delta_{C-N(O_2)}$ (13)
206	–	–	–	0.69	–	0.8	0.2	$\delta_{C-N(O)_2}$ (62)
192	–	–	–	0.74	–	0.6	1.3	γ_{CH_3} (22), $\delta_{C-N(O_2)}$ (21), γ_{CC} (12)
183	–	–	–	0.58	–	0.5	0.0	γ_{CH_3} (71)
104	–	–	–	0.75	–	0.5	0.6	γ_{CC} (56), $\delta_{C-N(O_2)}$ (14)
52	–	–	–	0.75	–	0.0	0.3	γ_{NO_2} (81), γ_{CC} (15)

Abbreviations: vs, very strong; s, strong; m, medium; w, weak; vw, very weak; sh, shoulder.

[a] A percentage contribution of each local mode to a given normal vibration is given in brackets.

[b] VV: vertical–vertical (parallel) and VH: vertical–horizontal (perpendicular) polarizations.

[c] Depolarization degree calculated at B3LYP/6-31++G(d,p) level.

[d] Depolarization degree determined from integrated intensities of the bands in the polarized Raman spectra of the MNA solution.

Experimental dichroism values were estimated as ratios of intensities measured at maximum heights of a given band in X and Z polarized spectra, respectively. The dichroic ratios calculated from OGM and observed for vibrational bands in spectra of the MNA crystal are collected in Table 2.

RESULTS AND DISCUSSION

Molecular and crystal structure of MNA

MNA crystallizes in the monoclinic crystal system, space group Ia (Cc), with four molecules per unit cell with the following lattice constants: $a = 7.589(3)$ Å, $b = 11.613(2)$ Å, $c = 8.231(4)$ Å, and $\beta = 94.09(7)^\circ$. The angle between benzene ring and nitro group amounts to 1.7°. The torsion angles H1A–N1–C1–C6 and H1B–N1–C1–C2 in the amine group are −5.68° and 9.14°, respectively. The amine group in the crystal reveals pseudo sp^3 hybridization in the electronic ground state, thus the interaction of its lone pair electrons with nearby π system of the aromatic ring seems to be rather weak. The nitro group is coplanar with the phenyl ring that enables electrons of this group to couple with π electrons of the ring. The calculated electric dipole moment of the free MNA molecule amounts to 7.9 D (7.6 D for p-NA molecule).[10] The dipole moment of the MNA molecule in a crystal has recently been reexamined and estimated as close to 11.3 D[23] while the value of 25 ± 8 D was reported previously.[22] The dipole moment of each molecule in a crystal is inclined with respect to the (010) plane and one molecule is slightly pointed up and another pointed down to the plane. These molecules are related by the glide plane which consists of the reflection through (010) plane and translation of $\frac{1}{2}\mathbf{a}$. Because of this reflection there is no dipole moment perpendicular to the (010) plane (along **b** axis). The polar axis lies in the (010) plane at an angle of 26.7° with respect to the **c** axis.[2]

There are several weak hydrogen bonds (HBs) in the MNA crystal. The shortest intermolecular distances

DOI: 10.1002/jrs

Table 2. Proposed assignments of bands to normal vibrations of MNA molecule in crystal

IR										
Crystal, polarization [cm^{-1}]		MNA in KBr	DMNA in KBr	Raman, powdered samples [cm^{-1}]		IINS [cm^{-1}]	Dichroic ratio $R_{X/Z}$		Assignment	
~||Z	~||X	pellet [cm^{-1}]	pellet [cm^{-1}]	MNA	DMNA		Calc.[a]	Exp.[b]		
1	**2**	**3**	**4**	**5**	**6**	**7**	**8**	**9**	**10**	
3472vs	3472vs	3470vs	3472w	3474m	–	–	∞	~1	$\nu^{as}_{NH_2}$	
~3416 vw	–	–	3439w	–	–	–	–	–	–	
3369w	3384[c]	3362vs	3439w	3364vs	–	–	∞	≫1	$\nu^{s}_{NH_2}$	} F.r.
–	–	–	3365m, 3390w[d]	–	–	–	–	–	$2\delta^{s}_{NH_2}$	
–	3243[c]	3249m	3249vw	–	–	–	–	–	–	
~3225 vw	–	3236m	–	–	–	–	–	–	–	
–	3189w	–	–	–	–	–	–	–	–	
–	3099w	–	3098vw	–	–	–	**30.5**	∞	ν_{CH} (20b)	
3071m	3071m	3070vw	3071w	–	–	–	**30.5**	>1	ν_{CH} (20a)	
3045w	3044vvw	–	–	–	–	–	**30.5**	0	ν_{CH} (2)	
2987w	2987w	2985vw	2986w	–	–	–	–	~1	$\nu^{as}_{CH_3}$[e]	
2967sh	2969w	–	–	–	–	–	–	–	ν_{CH_3}	
2943s	2943sh	2942vw	2944w	–	–	–	–	≪1	$\nu^{as}_{CH_3}$	
2907w	2909m	2901vw	–	–	–	–	–	–	$\nu^{as}_{CH_3}$	
2894w	2891w	–	2898w	–	–	–	–	–	$2\delta^{as}_{CH_3}$	
2852m	2861m	2860s	2958w	–	–	–	–	–	ν_{CH_3}	
–	–	–	2602m	–	2607vvw	–	–	–	$\nu^{as}_{ND_2}$	
–	–	–	2447m	–	2451w	–	–	–	$\nu^{s}_{ND_2}$	
–	1634w	1634s	1634vw	–	–	–	∞	≫1	$\delta^{s}_{NH_2}$	
1609w		1603m	1604s	–	1601vw	–	**30.5**	–	ν_{CC} (8b)	
1589vw	~1602[c]	1584s	1580s	1584vw	1581vw	–	**30.5**	–	ν_{CC} (8a)	
1545m		–	1556sh	–	–	–	–	–	$2\gamma_{CH}$ (11)	
–	1513m	–	–	–	–	–	–	≫1	?	
1509vw	1505m	1509s	1506s	1507vw	1511w	–	**9.30**	≫1	$\nu^{as}_{NO_2}$	
1481m	1477m	1474s	1478s	–	1480vvw	–	**30.5**	<1	ν_{CC} (19b)	
1454s	1449m	1456m	1457s	–	–	–	–	≪1	$\delta^{as}_{CH_3}$	
1440s	1436m	1437w	1427s	–	1430	–	–	≪1	$\delta^{as}_{CH_3}$	
1418vw	1420m	1418m	1415sh	–	–	–	–	>1	δ_{CH_3}	
1385w	1385m	1386w	1385w	–	–	–	**30.5**	~2	ν_{CC}	
1360m	1360m	1358sh	1358w	1356m	–	–	–	~1	$\delta^{s}_{CH_3}$	
1333w		–	1345w	1333m	1338sh	–	**37.6**	0	$\nu^{s}_{NO_2}$	
–		1312sh	1314sh	1311sh	1312sh	–	**30.5**	–	$\delta_{CH}(3) + \nu_{C-NO_2}$	
–		–	1294s	–	–	–	–	–	?	
–	~1282[c]	1291vs	1283s	1289vs	1295vs,1285vs[d]	–	**30.5**	–	ν_{C-NH_2}	
1267w		1263vs	1263s	1265vs	1267vs	–	**30.5**	≫1	ν_{CC} (14)	
–		1248sh	1244sh	–	1248sh	–	–	–	?	
1207w	1206s	1204m	1194vs	1203m	1197s	–	**30.5**	~1	ν_{C-CH_3}	
1154m	1153s	1152s	1157w	1152m	1149vw	–	**30.5**	>1	δ_{CH} (15)	
–	1140sh	–	1145w	–	–	–	–	–	–	
–	–	–	1119sh	–	–	–	–	–	$\delta^{s}_{ND_2}$	
–	1103s	1095vs	1090vs	1098m	1092m	–	**30.5**	–	δ_{CH} (18b)	
–	–	1053sh	–	1053w	–	–	∞	–	$\delta^{as}_{NH_2}$?	
1036s	1037s	1035m	1035w	–	–	–	–	–	δ_{CH_3}	
–	1010s	1009m	1008w	1009vw	1011w	–	**30.5**	>1	ν_{C-NO_2} ?	
–	–	–	982sh	–	–	–	–	–	–	

Table 2. (*Continued*)

IR									
Crystal, polarization [cm^{-1}]		MNA in KBr	DMNA in KBr	Raman, powdered samples [cm^{-1}]		IINS [cm^{-1}]	Dichroic ratio $R_{X/Z}$		Assignment
$\sim\|\|Z$	$\sim\|\|X$	pellet [cm^{-1}]	pellet [cm^{-1}]	MNA	DMNA		Calc.[a]	Exp.[b]	
1	**2**	**3**	**4**	**5**	**6**	**7**	**8**	**9**	**10**
966vw	964	960sh	953vw	–	966vw	–	**0.02**	≫1	$\gamma_{CC}(4) + \gamma_{CH}$ (10a)
932vw	932	930sh	939w	933m	944m	–	**30.5**	–	ν_{C-NO_2}
896vs	896s	895s	896vw	895w	898vw	–	**0.02**	~1	γ_{CH} (10b)
–	–	846sh	850w	–	859m	–	**30.4**	–	$\delta^{s}_{NO_2}$
825vs	823s	825s	824vs	–	824vw	–	**0.80**	~1	$\gamma_{CH}(11) + \gamma_{C-NH_2}$
816sh	–	816sh	–	814s	815m, 810m[d]	–	**20.2**	–	$\delta^{s}_{NO_2}$
–	–	–	805w	–	–	–	–	–	–
–	772s	771vw	–	771s	–	779w	**0**	∞	γ_{NH_2} (wag)
–	–	–	–	–	764m	–	–	–	–
753vs	751s	752s	753vs	752vs	–	–	**0.80**	<1	γ_{NO_2} (wag)
716vs	715	714m	715w	–	–	730w	**0.02**	<1	γ_{CC} (16b)
646vw	645vs	644m	640s	644m	644w	–	**30.5**	≫1	δ_{CC} (6a)
–	599w	–	–	–	–	608m	–	–	?
–	556w	555m	–	553m	549w	–	**30.4**	>1	$\delta^{as}_{NO_2}$
540w	540s	539vw	547s	539m	–	542m	**30.5**	≫1	$\delta_{CC}(1) + \delta_{C-CH_3}$
529w	–	529vw	529w	–	534w	–	**0.02**	–	γ_{CC} ?
–	~498w	–	493sh	–	–	504m	–	–	–
–	–	–	–	–	–	478s	–	–	–
–	–	448m	–	–	–	445m	**0.8**	–	γ_{NO_2} (inv)
–	–	–	454w	–	–	–	–	–	–
439w	442m	~430s	436w	433vs	–	430	**0.02**	>1	γ_{CC} (16a)
423w	422m	421sh	400w	422s	–	–	**30.5**	>1	δ_{C-NH_2}
391w	~4000 sh	–	–	–	–	–	–	–	?
380w	–	–	–	–	–	–	–	–	?
375m	376m	377vw	373sh	365w	374w	377w	**30.5**	~1	δ_{CC} (6b)
–	–	–	366sh	–	361vw	–	–	–	–
–	–	–	338vs	–	331w	333s	**0**	–	γ_{NH_2} (twist)
–	–	327w	–	326w	–	321s	**30.5**	–	δ_{CC} (12)
–	–	280vw	281vw	–	–	–	**0.02**	–	γ_{C-NO_2}
–	–	–	–	–	–	258vs	–	–	γ_{CH_3}
–	–	–	–	–	–	230sh	–	–	–
–	–	225w	225vw	224vw	225vw	221s	–	–	γ_{C-CH_3}
–	–	212w	211w	212w	214vw	–	**30.5**	–	δ_{C-NO_2}
–	–	–	204sh	–	–	–	–	–	–
–	–	151vw	148vw	–	–	154m	**0**	–	γ_{C-NH_2}
–	–	–	–	136m	137w	131m	–	–	?
–	–	141vw	141vw	–	–	–	–	–	$2\gamma_{NO_2}$
–	–	123vw	122vw	–	123w	127m	–	–	Ring torsion

N1–H1B···O2 and N1–H1A···O1 amount to 3.097 and 3.246 Å (Fig. 11, and Table 3), respectively. The amine and the nitro groups act as double proton donor and a double proton acceptor, respectively, in the N–H···O type HBs (*cf* Fig. 11). Additionally, each methyl group interacts with oxygen atoms from molecules of the closest layers, serving as a double proton donor in C–H···O contacts. The H7C atom of the methyl is at the distance of 1.90 Å from H1B atom of the amine group of the same molecule. This distance lies in the range of 1.7–2.2 Å, typical for

DOI: 10.1002/jrs

Table 2. (*Continued*)

IR									
Crystal, polarization [cm^{-1}]		MNA in KBr	DMNA in KBr	Raman, powdered samples [cm^{-1}]			Dichroic ratio $R_{X/Z}$		
~||Z	~||X	pellet [cm^{-1}]	pellet [cm^{-1}]	MNA	DMNA	IINS [cm^{-1}]	Calc.[a]	Exp.[b]	Assignment
1	**2**	**3**	**4**	**5**	**6**	**7**	**8**	**9**	**10**
–	–	94w	94w	–	–	105m	–	–	Lattice
–	–	85vw	84w, 80w[d]	88s	89s	–	**0.8**	–	γ_{NO_2}
–	–	72vw	72w	72s	70s	~80 m	–	–	lattice
–	–	60vw	64w	60vs	61vs	–	–	–	lattice
–	–	–	55w	45s	47s	~54 m	–	–	lattice

Abbreviations: vs, very strong; s, strong; m, medium; w, weak; vw, very weak; sh, shoulder; F.r., Fermi resonance.
The numbers in brackets are Willson's notation of benzene ring vibrations.
[a] Dichroic ratio calculated on the basis of OGM.
[b] Experimental dichroic ratio estimated from polarized IR spectra of MNA crystal.
[c] Position of the gravity center.
[d] Doublet.
[e] According to[28].
Wavenumbers below 400 cm^{-1} in columns 3 and 4 are taken from the spectra of MNA and DMNA in nujol suspension, respectively.

Table 3. The geometry of the shortest intermolecular contacts in the MNA crystal. The last row displays the shortest intramolecular H···H interaction

	X-H···Y (Å)	H···Y (Å)	X···Y (Å)	X-H···Y angle (°)
1	N1–H1B^{i}···O2^{ii}	2.18(8)	3.097(8)	167(6)
2	N1–H1A^{i}···O1^{iii}	2.52(7)	3.246(7)	142(6)
3	C6–H6^{i}···1^{iii}	2.63(6)	3.466(7)	139(4)
4	C7–H7A^{i}···O1^{iv}	2.66(6)	3.430(9)	140(4)
5	C7–H7C^{i}···O2^{ii}	2.53(7)	3.253(8)	131(5)
6	C7–H7A^{i}···C3^{iv}	3.39(6)	3.953(9)	121(4)
7	C7–H7B^{i}···π (Ph)^{v}	3.08	3.727	125
8	C7–H7C^{i}···H1B^{i}-N1	1.90(4)	2.50(4)	117(3)

Symmetry codes: (i) x, y, z; (ii) 0.5 + x, −y, 1 + z; (iii) 0.5 + x, 0.5 + y, 0.5 + z; (iv) x, −0.5 − y, 0.5 + z; (v) −0.5 + x, −y, z.

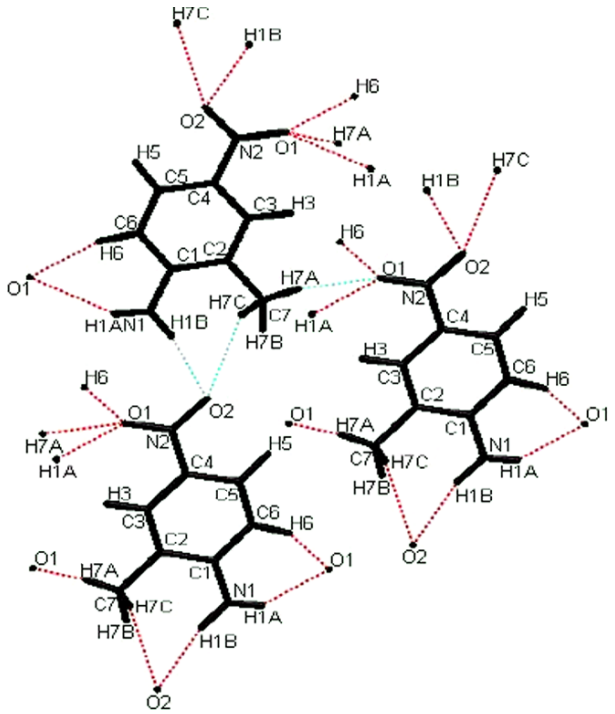

Figure 11. The shortest intermolecular interactions in the MNA crystal. View along the **a** axis. This figure is available in colour online at www.interscience.wiley.com/journal/jrs.

so called dihydrogen bonds.[31,32] There is also another C–H···O contact which involves the phenyl H6 hydrogen. The $CH_3 \cdots \pi$(Ph) interaction between the molecules is also found. Summarizing, each MNA molecule in the crystal has many close contacts with neighboring molecules. This number rises if one takes into account five H···H contacts (2.39–2.72 Å), which are also considered as interactions which direct crystal packing in aromatic hydrocarbons to one of the four main patterns (herringbone, β, γ, or sandwich-herringbone).[33,34] A stacking pattern is created by the MNA molecules. All these contacts enable to form a zigzag of polar molecules[4] and to create the polar axis P at about 8° angle with respect to the X dielectric axis[2] (Fig. 1).

ANALYSIS OF BANDS WAVENUMBERS AND INTENSITIES IN THE FREE MOLECULE AND IN THE MOLECULE IN CRYSTAL

Benzene ring vibrations

The increase of vibrational wavenumbers of the out-of-plane bending γ_{CH}, the decrease of the stretching ν_{CC} modes and the decrease of the stretching ν_{CH} bands intensities in the IR spectra, as compared with those of the parent hydrocarbon, occur when the phenyl group in a given derivative behaves as an electron donor.[12,14] In the case of IR spectra of MNA the wavenumbers of one stretching ν_{CC} (8b) and of three out-of-plane bending γ_{CH} (10a, 10b, 11) vibrations are higher than the corresponding ones in the benzene molecule (taken from Ref. 27), namely: 1608 *vs* 1599, 960 *vs* 846, 895 *vs* 846, and 825 *vs* 673 cm^{-1} (first number denotes the wavenumber of a given vibration in the MNA molecule while the second gives the corresponding wavenumber in benzene). Positions of the three stretching ν_{CC} (8a, 19a, 14) vibrational bands in the IR spectrum of the MNA molecule in a crystal are lower than those in benzene: 1584 *vs* 1599, 1385 *vs* 1482, 1265 *vs* 1409 cm^{-1}. The IR intensities of the stretching ν_{CH} bands at about 3100 cm^{-1} are smaller in MNA solutions and crystal compared with those of corresponding benzene bands (in the IR spectra of benzene solution in $CHCl_3$ not shown here). These features reflect stronger electron donor than electron acceptor properties of the benzene ring in solid MNA. It is in line with the positive value of a charge on the benzene ring in the MNA molecule in crystal reported by Whitten *et al*.[23]

$-NH_2$ and $-NO_2$ vibrations

The $\nu^{as}_{NH_2}$ band lies about 40 cm^{-1} lower in the infrared spectra of the MNA crystal than those in MNA in solutions (Tables 1 and 2). In both X and Z polarized IR spectra of MNA the shape of this band is typical for crystals with very weak HBs.[35] The strong and broad band (massif) of the symmetric stretching vibration of the amine group, $\nu^{s}_{NH_2}$, ($\Delta\nu_{1/2} \approx 300$ cm^{-1}) in the X polarized spectrum has the center of gravity red shifted of about 170 cm^{-1} in comparison to the spectrum of solution, and it lies 22 cm^{-1} lower than in the Z polarized spectrum. It is in accord with the two distinct NH···O hydrogen bonds lying in different directions with the shortest one parallel to the X direction (*cf* Figs 1, 2, and 11). Fermi resonance between the $\nu^{s}_{NH_2}$ vibration and the first overtone of $\delta^{s}_{NH_2}$ vibration at about 3200 cm^{-1} contributes to the intensity of the $\nu^{s}_{NH_2}$ massif. The differences between $\nu^{as}_{NH_2}$ and $\nu^{s}_{NH_2}$ values, $\Delta(\nu^{as} - \nu^{s})$, grow when the HNH angle increases what in turn is a measure of a charge decrease on the $-NH_2$ group.[27] $\Delta(\nu^{as} - \nu^{s})$ values are equal to 98 and 110 cm^{-1} for the bands found in the X and Z polarized IR spectra of the MNA crystal and to 94 cm^{-1} for these bands in the solution spectra. It suggests decrease of a negative charge on the $-NH_2$ group in crystal in accord with the conclusions in Ref. 23.

Very strong intensities of the bands of out-of-plane bending (γ) modes of the benzene ring as well as of the $-NH_2$ and $-NO_2$ groups in the Raman spectra of polycrystalline MNA (Fig. 6) and in the Z polarized IR spectra of the MNA crystal (Table 2, Fig. 3, see 700–1100 cm^{-1} range) can be due to intermolecular $\pi-\pi$ interactions. π orbitals of benzene rings lie actually along the Z direction. The smallest distance between the phenyl rings forming one stack does not exceed 3.5 ´Å, however there is a 1.7 ´Å offset of the neighboring rings. Repulsion between π electrons of neighboring molecules increases electrostatic interactions along the Z direction making the IR bands of out-of-plane vibrations intensive. Strong intensities of these bands also in the Raman spectra suggest that these $\pi-\pi$ interactions cause some kind of electron–phonon couplings. It is partially in accord with the suggestion of Vallée *et al*.[6] that these interactions are the strongest ones in the MNA crystals. In our opinion the HBs are the most important interactions.

Methyl group vibrations

One of C–H bonds of the methyl group in the MNA molecule in the crystal lies in the benzene ring plane. Thus the symmetric C–H stretching vibration should be polarized parallelly and the antisymmetric vibration perpendicularly to the benzene ring plane.[28] In our IR experiment these directions correspond to the X (actually XY plane) and Z polarizations, respectively. There are several bands that we have assigned to two stretching (symmetric and antisymmetric) vibrations of the methyl (see Table 1). One of them, at 2943 cm^{-1}, is intensive, complex and polarized along the Z direction. The rest of the bands are polarized along the X axis what must result from numerous bondings in which the methyl group is involved. The broadness of all stretching bands is also the manifestation of C–H···O bondings. Additionally, there are 5 and 4 cm^{-1} differences between positions of bands of two bending $\delta^{as}_{CH_3}$ vibrations in X and Z polarized spectra. We suppose that these are Davydov splittings. On the other hand, positions of the mentioned methyl group bending vibrations bands in the MNA crystal (Table 2) are distinct from those in solution (Table 1). Thus, it can not be excluded that it is not the excited dipole–excited dipole interactions but the intramolecular C–H···H–N interaction and intermolecular C–H···O bondings that are responsible for differences. Davydov splittings were not observed in the IR spectra of MNA deposited on PTFE.[6] The absence of stretching vibration bands of the methyl in the spectra of solutions did not allow us to adjudicate whether the above mentioned vibrations are red or blue shifted in crystal due to C–H···H–N and C–H···O bonds formation.

Lattice and low wavenumber vibrations

Vibrational bands from the region below 450 cm^{-1} are not well defined by the chemical quantum calculations due to the fact that in this wavenumber range internal rotations of substituent groups and deformations of a molecule are affected by its external vibrations (librations and translations) whereas the calculations are performed for the molecule in a

DOI: 10.1002/jrs

gas phase. In assigning vibrations to bands in this region, first of all we have taken into account the IINS spectra (Fig. 9). The IINS technique is a powerful method for analyzing modes with participation of H-atoms due to the large neutron scattering cross-section of hydrogens as well as of carbon atoms.[36]

The most intense band at 258 cm^{-1} in the IINS spectrum measured at 20 K is supposed to originate from the torsion of the methyl substituent (Table 2) in which there is the largest concentration of hydrogen atoms in the MNA molecule. This band is neither observed in the IR spectrum of MNA suspension in nujol nor in the Raman spectrum of powdered MNA (Figs 6 and 7, respectively). Other two strong bands at 221 and 333 cm^{-1} in the IINS spectrum, are assigned to the γ_{C-CH_3} and γ_{NH_2} (twist) vibrations, respectively.

The deuteration practically does not change positions and relative intensities of six vibrational bands below 150 cm^{-1} (Table 2, Figs 5 and 6). Among them, four are lattice vibration bands, thus it can be concluded that not only NH – O hydrogen bonds play a role in the crystal structure stabilization, but also other HBs that remain unaltered after deuteration.

HYDROGEN BONDS

Formation of NH···O bonds in the MNA crystal results in the polarization of the electron charge distribution: the $-NO_2$ group becomes slightly more negative (by 0.07 e) and the $-NH_2$ group less negative (by the same 0.07 e value) in comparison with charges in the free molecule.[23]The large intensity of the 3100–3400 cm^{-1} massif connected with the hydrogen bonded amine stretching $\nu^s_{NH\,2}$ vibration in the X direction reflects the polarization of the N–H bond. The C–H···N–H interaction also polarizes one of N–H bonds along the X direction. The C7–H7C···O2 hydrogen bonding lowers the wavenumber of the symmetric stretching of the $-NO_2$ group in the crystal (1333 cm^{-1}) in the comparison with analogical vibration in deuterated MNA (1345 cm^{-1}). The out-of-plane deformation vibration of the $-NH_2$ oscillator participating in HB, $\gamma_{NH\cdots O}$, corresponds to the 200–700 cm^{-1} massif. It appears both in the infrared spectrum of MNA in KBr pellet and in the polarized IR spectra measured with the beam polarized along X, Z and intermediate directions (not shown in here). After deuteration the center of gravity of the massif shifts from ~460 to ~330 cm^{-1} and the band becomes narrower. It was difficult to find the bands of ν^s_{NO2} and ν^{as}_{NO2} vibrations in the Raman spectra of powder and in the polarized IR spectra. The band of ν^{as}_{NO2} vibration in the IR spectra is weak and polarized along the Y direction. The band of ν^s_{NO2} vibration is a part of a large ~700–1400 cm^{-1} massif in the X polarization (*cf* Table 2 and Fig. 3). Large intensity of the massif is connected with several intermolecular HBs in crystal (Table 3). Some spectral manifestations of C–H···H–N and C–H···O HBs were signalized in section concerning methyl group vibrations. In the X polarized IR spectra there are yet, strong and broad bands appearing at 2716 and 2738 cm^{-1}. We suppose that they represent the C–H···O bridge vibrations.

Several H···H interactions in the MNA crystal have their direction along the Z axis (they are created between neighboring molecules). As their character is considered as predominantly electrostatic[32] they enhance only the polarizability along Z direction, but do not influence the spectra as typical HBs do.

APPLICABILITY OF ORIENTED GAS MODEL

Among 26 pairs of predicted and experimentally determined dichroic ratio values ($R_{X/Z}$) 15 are in good agreement and for three pairs the values of $R_{X/Z}$ ratios can be considered as similar (e.g. for the stretching ν_{CC} (19a) vibration the theoretical value equals to 30.5 whereas the experimental one is about 2).

Experimental *vs* calculated values of dichroic ratios are convergent for substituent vibrations and do not agree one with another in the case of few out-of-plane bending vibrations of the phenyl ring (Table 2). It means that in OGM, tdm of a three atomic oscillator are better approximated than tdm of the six-atomic ring. Intra- and intermolecular interactions do not strongly affect the vibrations of substituents in the MNA molecule in crystal, but they influence vibrations of the ring by changing the predicted tdm's. As the geometry of the molecule in crystal does not differ significantly from that found from *ab initio* calculations, the nonbonding interactions in the crystal are the cause of changes in tdm in molecule. Also delocalization of many normal modes into numerous atoms can lead to discrepancies from OGM. The dispersion of dielectric axes, possible in monoclinic crystals, was not considered as the consecutive reason of the differences in $R_{X/Z}$ values because dependences of the refractive indices in MNA crystal on the wavelength reveal monotonic decreases.[30]

ELECTRONIC TRANSITIONS IN THE MNA MOLECULE IN SOLUTIONS AND IN CRYSTAL. VIBRONIC COUPLINGS

Bands in the region 50 000–20 000 cm^{-1} in the electronic spectra of the solid MNA (Fig. 8) are mainly due to intramolecular electronic transitions propagating in crystals as excitons. However there are two bands, at 16 530 and 15 750 cm^{-1}, with small oscillator strengths, which are related to intermolecular charge transfers (CTs) predicted by calculations[9]. High anisotropy observed in the polarized IR spectra of the MNA crystal (Fig. 10) and the enhancement of intensities of bands along the X direction is analogical to the anisotropy found in the polarized reflectance and electroreflectance spectra[8] and reveals vibronic couplings in the MNA crystal. According to Tokura *et al*.[8] the strongest ICT band at about 21 730 cm^{-1} appears in the X polarized spectra of both

DOI: 10.1002/jrs

types. In the reflection spectra measured without external electric field no bands were found in the Z polarized spectra. After applying the a.c. electric field of 8.7 kV cm^{-1} two weak bands appeared also in this direction.[8] This fact supports our statement about $\pi-\pi$ interactions in the Z direction.

On the basis of the measured UV-Vis spectra the differences, $\Delta\nu_{el}$, between the first electronic transition in MNA crystal or solutions and the forbidden $B_{2u} \leftarrow A_{1g}$ transition in benzene molecule in the gas phase at 38089 cm^{-1} have been calculated. This difference was introduced as a measure of benzene derivative's ability for the ICT and for vibronic couplings[11,12,14]. The $\Delta\nu_{el}$ values amount to ~7200 cm^{-1} for MNA in the isooctane solution, ~13 100 cm^{-1} in water, and ~16 600 cm^{-1} for the MNA molecule in the crystal. For the comparison, $\Delta\nu_{el}$ values calculated for the p-NA molecule in water amount to 12 500 cm^{-1} and 16 500 cm^{-1} for this molecule in the crystal[37] indicating that they are very similar in both materials. The largest $\Delta\nu_{el}$ value obtained for the MNA molecule in the crystal explains very strong IR intensities of bands in the X polarized spectrum of the MNA crystal in comparison with the spectra of solutions, what is in accord with the theory of IR bands intensities.[15] In the case of MNA solutions in nonpolar and aprotic solvents the $\Delta\nu_{el}$ is connected with ICT; however in crystals it is the result of both intra- and intermolecular charge transfers. Since we do not observe any shortening in neither of the C–N(H) nor the C–N(O) bond lengths, we suppose that in the crystal mainly intermolecular charge transfers take place. It explains why symmetric and antisymmetric stretching vibrations of the amine group and the symmetric stretching vibration of the nitro group possess strong intensities along the same, X direction. In the IR spectra of MNA solutions (Fig. 4) the situation is different and the ICT from the phenyl ring to the nitro group causes that the symmetric stretching vibration band of the nitro group is the strongest one in the IR spectrum, while the amine stretching bands are rather weak and slightly broadened.

The noticeable enhancement of the nonlinear optical (NLO) response due to the concerted interactions of ICT and HBs was found in urea[38] and in the m-aminophenol[11] crystals. It seems that the MNA crystal HBs enable intermolecular charge transfers.[9,23]The observed 4–6 cm^{-1} Davydov splittings of some bands (Table 2) and LO-TO gaps, calculated from Ref. 7 data, ranging up to 20 cm^{-1} indicate that the excited dipole–excited dipole and long range dipole–dipole interactions play also significant role in MNA crystals. These values as well as the averaged MNA reflectivity of 20%,[7] are similar to those reported for m-NA crystals[12,13] and they suggest the weak conductivity of MNA crystals.

The most intense absorption continua (massifs) appear in the X polarized IR spectra and their intensities decrease when rotating polarizer toward the Z direction. Three of them, in the MIR region: 3400–3100, 1400–700, and 700–200 cm^{-1} have already been discussed; they originate from hydrogen bonded $-NH_2$, $-NO_2$, and $-CH_3$ oscillators coupled with intermolecular CTs. In the NIR region in the X polarized spectra (Fig. 10) there are yet two large massifs with maxima at about 4300 and 6600 cm^{-1}. Their appearance can be connected with intermolecular electron density transitions. Such effect is supported by Guillaume *et al*.[9] calculations according to which the increase of MNA unit cells size along the given crystallographic direction causes the decrease of intermolecular CT energy. The most pronounced decrease takes place along the **a** axis (the **c** axis in our structure) which is near to the X direction (Fig. 1). On the other hand the presence of ion radicals, with the concentration 6×10^{15} spins per gram at the room temperature, has been revealed by EPR for the powdered MNA. Such little amount of ion radicals, charge carriers, can appear due to the HB's breaking and/or due to crystal defects. Thus, we consider electronic transitions of radical anions to be responsible for the large bands in the NIR region. The doublet–doublet, D_0-D_1, transition energy (12 500 cm^{-1}) between the radical anion states in the MNA molecule calculated in Ref. 10 is lower than the energy of a singlet–triplet S_0-T_1 transition of the closed shell molecule and this effect may be much smaller in the crystal. Similar NIR electronic transitions were observed in polyacene radical anions,[17] semiquinone radical anions,[39] and positively charged radical π–dimers spectra.[40]

CONCLUSIONS

The analysis of vibrational wavenumbers and intensities together with the study of electronic absorption spectra revealed the strong anisotropic intermolecular interactions in the MNA crystals. Two NH···O, three CH···O and intramolecular CH···HN short contacts were found between and inside MNA molecules in crystal. The contacts not only stabilize the crystal structure, but also, instead of the ICT, enable CT between neighboring molecules. The geometry of these interactions builds up the polar axis causing strong anisotropy of infrared absorption. The presence of ion radicals, of various origin, in the MNA crystals is responsible for two unusually large bands in the X polarized NIR spectrum. The $\pi-\pi$ offset stacking interactions along the Z direction enhance the intensity of out-of-plane bending vibrational bands. The substitution of a methyl group to the p-NA molecule results in the crystallization of MNA in the non-centrosymmetric Ia space group and leads to formation of the weak C–H···O and CH···HN hydrogen bonds. These bondings stabilize the sheet motif of the MNA molecules. The $CH_3\cdots\pi$ (Ph) and the weak H···H interactions stabilize the stacked structure.

Acknowledgements

This work was sponsored in part by Polish Academy of Science, grant no. 3 T08A 08 229. Calculations have been performed in Wroclaw Centre for Networking and Supercomputing (WCSS). The help of Professor Krystyna Dyrek and Dr Ewa Bidzińska from Jagiellonian University in Cracow regarding EPR studies is kindly acknowledged.

REFERENCES

1. Levine BF, Bethea CG, Thurmond CD, Lynch RT, Bernstein JL. *J. Appl. Phys.* 1979; **50**: 2535.
2. Lipscomb GF, Garito AF, Narang RS. *J. Chem. Phys.* 1981; **75**: 1509.
3. Zyss J. *J. Non-Cryst. Solids* 1982; **47**: 211.
4. Ferguson G, Glidewell C, Low JN, Skakle JMS, Wardell JL. *Acta Cryst.* 2001; **C57**: 315.
5. Vallée R, Damman P, Dosiere M, Toussaere E, Zyss J. *J. Am. Chem. Soc.* 2000; **122**: 6701.
6. Vallée R, Damman P, Dosiere M, Scalmani G, Bredas J. *J. Phys. Chem.* 2001; **105**: 6064.
7. Nogueira EMD, de Gomes E, Belsley MS, Lancere-Mendez S, Cunha JM, Vega A, Mano JF. *Solid State Sci.* 2001; **3**: 733.
8. Tokura Y, Kurita A, Koda T. *Phys. Rev. B* 1985; **31**: 2588.
9. Guillaume M, Botek E, Champagne B, Castet F, Ducasse L. *Int. J. Quantum Chem.* 2002; **90**: 1378.
10. Szostak MM, Kozankiewicz B, Lipiński J. *Spectrochim. Acta* 2007; **67**: 1412.
11. Szostak MM, Germańska J, Kowala A. *J. Mol. Struct.* 1990; **222**: 285.
12. Szostak MM. *Chem. Phys.* 1988; **121**: 449.
13. Szostak MM, Le Calvé N, Romain F, Pasquier B. *Chem. Phys.* 1994; **187**: 373.
14. Szostak MM, Misiaszek T, Roszak S, Rankin JG, Czernuszewicz RS. *J. Phys. Chem.* 1995; **99**: 14992.
15. Mizuno M. *Spectrochim. Acta* 1978; **34A**: 947.
16. Albrecht A. *J. Chem. Phys.* 1961; **34**: 1118.
17. Wiesman JL, Mattioda A, Lee TJ, Hudgins DM, Allamandda LJ, Bauschlicher Jr. CW, Head-Gordon M. *Phys. Chem. Chem. Phys.* 2005; **7**: 109.
18. Szostak MM, Jakubowski B, Komorowska M. *Mol. Cryst. Liq. Cryst.* 1993; **229**: 7.
19. Szostak MM, Wójcik G, Gallier J, Bertault M, Freundlich P, Kolodziej HA. *Chem. Phys.* 1998; **229**: 275.
20. Szostak MM, Kozankiewicz B, Wojcik G, Lipiński J. *J. Chem. Soc., Faraday Trans.* 1998; **94**: 3241.
21. Szostak MM, Czarnecki MA. *Pol. J. Chem.* 2002; **76**: 419.
22. Howard ST, Hursthouse MB, Lehmann CW, Mallinson PR, Frampton CS. *J. Chem. Phys.* 1992; **97**: 5616.
23. Whitten AE, Turner P, Klooster WT, Piltz RO, Spackman MA. *J. Phys. Chem. A* 2006; **110**: 8776.
24. Hartshorne NH, Stuart A. *Crystals and Polarising Microscope*. Edward Arnold: London, 1960.
25. Frisch MJ, Trucks GW, Schlegel HB, Scuseria GE, Robb MA, Cheeseman JR, Montgomery Jr. JA, Vreven T, Kudin KN, Burant JC, Millam JM, Iyengar SS, Tomasi J, Barone V, Mennucci B, Cossi M, Scalmani G, Rega N, Petersson GA, Nakatsuji H, Hada M, Ehara M, Toyota K, Fukuda R, Hasegawa J, Ishida M, Nakajima T, Honda Y, Kitao O, Nakai H, Klene M, Li X, Knox JE, Hratchian HP, Cross JB, Bakken V, Adamo C, Jaramillo J, Gomperts R, Stratmann RE, Yazyev O, Austin AJ, Cammi R, Pomelli C, Ochterski JW, Ayala PY, Morokuma K, Voth GA, Salvador P, Dannenberg JJ, Zakrzewski VG, Dapprich S, Daniels AD, Strain MC, Farkas O, Malick DK, Rabuck AD, Raghavachari K, Foresman JB, Ortiz JV, Cui Q, Baboul AG, Clifford S, Cioslowski J, Stefanov BB, Liu G, Liashenko A, Piskorz P, Komaromi I, Martin RL, Fox DJ, Keith T, Al-Laham MA, Peng CY, Nanayakkara A, Challacombe M, Gill PMW, Johnson B, Chen W, Wong MW, Gonzalez C, Pople JA. *Gaussian 03, Revision C.02*, Gaussian: Wallingford, 2004.
26. Scott AP, Radom L. *J. Phys. Chem.* 1996; **100**: 16502.
27. Varsányi G. *Vibrational Spectra of Benzene Derivatives*. Akadémiai Kiadó: Budapest, 1969.
28. Moszyńska-Mierzecka B. DSc. Dissertation, Warsaw Technical University: 1978; (in Polish).
29. Rohleder JW, Luty T. *Molecular Crystals* 1968; **5**: 145.
30. Morita R, Ongasawara N, Umegaki S, Ito R. *Jpn. J. Appl. Phys.* 1987; **26**: L 1711.
31. Crabtree RH, Siegbahn PEM, Einstein O, Rheingold AL. *Acc. Chem. Res.* 1996; **29**: 348.
32. Grabowski SJ, Sokalski WA, Leszczyński J. *Chem. Phys.* 2007; **337**: 68.
33. Desiraju GR, Gavezotti A. *Acta Cryst. B* 1988; **44**: 427.
34. Desiraju GR, Gavezotti A. *Acta Cryst. B* 1989; **45**: 473.
35. Lautié A, Froment F, Novak A. *Spectr. Lett.* 1976; **9**: 289.
36. Pavlukojć A, Natkaniec I, Bator G, Sobczyk L, Grech E, Nowicka-Scheibe J. *Spectrochim. Acta A* 2006; **63**: 766.
37. Zych T, Misiaszek T, Szostak MM. *Chem. Phys.* 2007; **340**: 260.
38. Zyss J, Berthier G. *J. Chem. Phys.* 1982; **77**: 3635.
39. Józefiak TH, Miller LL. *J. Am. Chem. Soc.* 1987; **109**: 6560.
40. Small D, Zaitsev V, Jung Y, Rosokha SV, Head-Gordon M, Kochi KJ. *J. Am. Chem. Soc.* 2004; **126**: 13850.